

Tomographic Algorithm for Transverse Measurement of Multi-Core and Microstructured Optical Fibers

Andrew D. Yablon

*Interfiber Analysis, 8 Manns Hill Crescent, Sharon, MA 02067
andrew_yablon@interfiberanalysis.com*

Abstract: A new tomographic algorithm suitable for the transverse measurement of refractive index, residual stress, and spontaneous emission in multi-core and microstructured optical fibers is described and validated against several such fibers.

OCIS codes: (060.2270) Fiber characterization; (110.6960) Tomography

1. Introduction

Although transverse tomographic measurements have been extensively applied to measure refractive index [1-7], residual stress [5,8], and even transverse gain profile distribution of optical fibers [7], all previous implementations have been limited by a trade-off between the imaging depth-of-field and the spatial resolution. Sub- μm spatial resolution traditionally requires a high numerical aperture ($\text{NA} \sim 1.0$) imaging objective that inherently yields a depth of field on the order of $1 \mu\text{m}$ or less. Here I describe a new tomographic algorithm for combining transverse projections acquired at a multiplicity of angles and also at a multiplicity of focal positions that overcomes this limitation, thereby yielding high resolution ($\sim 1 \mu\text{m}$) over an enormous depth-of-field (many tens of μms). This new algorithm is particularly applicable to the measurement of multi-core and microstructured optical fibers, which contain fine structures distributed over large cross-sectional areas.

2. Data Acquisition and Processing Algorithm

A fiber sample is optically interrogated transversely through its side such that 1-dimensional projection data is acquired at a multiplicity of angular rotations and a multiplicity of focal positions. The previously described [6] experimental apparatus consisted of a Mach-Zehnder interference microscope that yields projections of optical path length as a function of transverse location. The algorithm described here is valid for any type of optical transverse projection data, including quantitative phase microscopy (QPM) [2,8], spontaneous emission [7], or beam diffraction angle [3], and may be used to measure refractive index, residual stress, or spontaneous emission.

The fiber sample is gripped by a rotation stage and discretely stepped through a complete rotation of 360° about its central axis in increments of 5° . At each of the 72 distinct rotation angles, 200 1-dimensional interferometric projections of the optical path length are recorded. These projections are acquired at video rate by a silicon CCD as the fiber is translated by a translation stage through the interferometer's imaging focal plane as shown in Fig. 1(a). During an 11 second long acquisition sequence, the fiber sample was translated approximately $260 \mu\text{m}$, so the approximate displacement of the fiber relative to the focal plane between each projection measurement was about $1.3 \mu\text{m}$. A completed acquisition sequence over all 72 rotation angles yielded $72 \times 200 = 14,400$ individual projections and required approximately 30 minutes.

Fig. 1(a) shows how the 1-dimensional projections of the optical path of a 3-core fiber vary as the fiber is moved through the focal plane. It is seen that any cores near to the focal plane are well-resolved whereas cores far from the focal plane are defocused, and, unfortunately, superposed with any focused features. Previous tomographic implementations [1-8] sought to acquire only one single projection at the center focal position (middle row of Fig. 1(a)) and as a result features far from fiber center were substantially smeared in the azimuthal direction. Isolating the focused information from the defocused information appears to be impossible. The new algorithm does not attempt to separate focused from defocused features, but instead relies on the fact that highly focused features are also highly localized and are therefore strongly reinforced so that they dominate over any diffuse contribution from defocused information.

A filter function that compensates for the conversion from transverse projections of a radial coordinate system into a Cartesian coordinate system [9] is convolved with each of the 14,400 recorded 1-dimensional projections. Then the individual, filtered, 1-dimensional projections acquired at distinct focal planes are assembled together into 2-dimensional matrices, one matrix for each of the 72 distinct rotation angles. These 72 2-dimensional matrices are then accumulated, with appropriate relative rotations as shown in Fig. 1(b), into a unified Cartesian coordinate system.

Image processing of the matrices was used to determine the correct center point for correctly registering the 2-dimensional matrices with respect to each other. The cladding edges of the fiber were automatically located to determine the transverse center of the fiber cladding. The axial center position (center focus) was determined from the 2-dimensional matrix by identifying the projection containing the sharpest cladding edges. Data processing required approximately 2 hours, but most of this time was associated with converting the phase images acquired by the interferometer into optical path length projections, and can be reduced significantly by more efficient computational schemes.

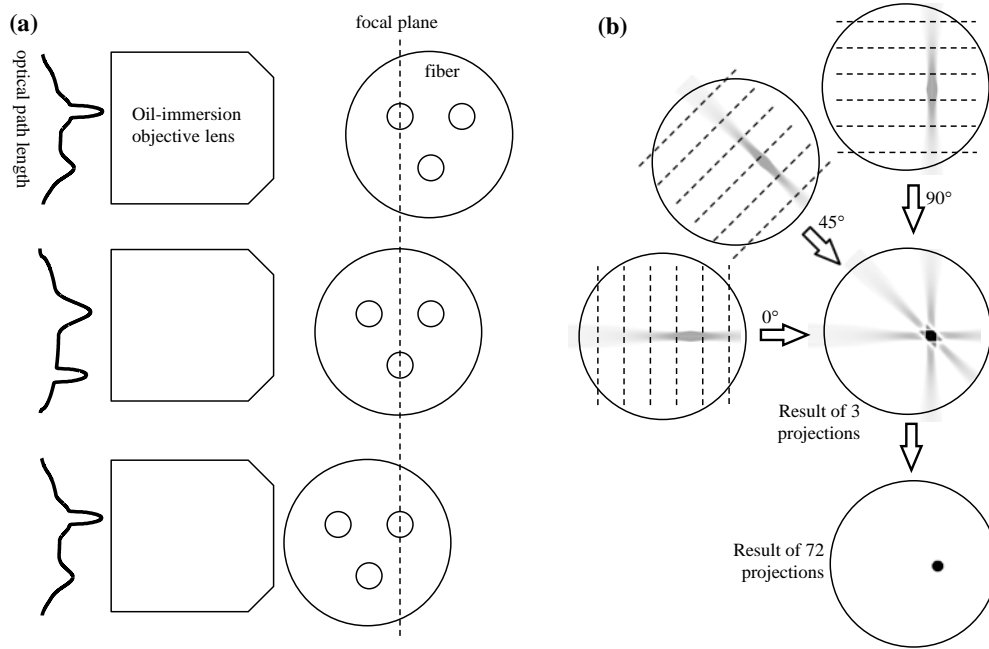


Fig. 1. At left (a) illustrates how the position of the focal plane affects transverse projections when the depth-of-field is small and how the fiber is translated through the focal plane to provide projection data at a multiplicity of focal positions. At right (b) illustrates how data acquired at a multiplicity of focal positions and at a multiplicity of angular orientations is superposed in a unified coordinate system to yield a high resolution rendition [10]. The grayscale images are representations of the 2-dimensional matrices assembled from an ordered set of (filtered) 1-dimensional projections. For clarity, only 3 representative angles are shown for a fiber with a single, off-center, core. Dashed lines correspond to distinct focal planes.

3. Results

Figure 2 shows results obtained using the new algorithm on a wide variety of multi-core and microstructured optical fibers. Note the general weakness of measurement artifacts despite the fact that the angular rotation step was a relatively coarse 5° . Fig. 2(a) depicts an 850 nm measurement of 4-core fiber provided by *Fibercore Ltd.* (FM 4C1500) that revealed refractive index dips in the center of the four cores (*inset*), even though all of the cores were about $35 \mu\text{m}$ from the fiber center.

Transverse optical measurements of air-silica microstructured fibers require the holes to be infused with a refractive index matching oil to reduce light refraction and scattering [3,4,8,10]. Fig. 2(b) depicts a 632.8 nm measurement of an endlessly single-mode air-silica microstructured fiber (*NKT Photonics* ESM-12B purchased from Thorlabs) and demonstrates the remarkable ability of the new algorithm to accurately render airholes as much as $47 \mu\text{m}$ from the fiber center. The airholes were all filled with an oil (*Cargille Labs* Series AA $n=1.454$) whose refractive index was accurately measured by the algorithm. No symmetry was assumed for the measurement of this evidently very symmetric fiber. The efficacy of the new algorithm is apparent from a comparison to previous efforts at measuring very similar fibers [3,8].

Figure 2(c) depicts a high-magnification view of 632.8 nm measurement of a polarization-maintaining (PM) air-silica microstructure optical fiber (*NKT Photonics* PM-1550 purchased from Thorlabs). As in the preceding sample, the airholes were infused with oil and the resulting refractive index contrast reveals the fiber's fine microstructure that contributes to form birefringence.

Figure 2(d) depicts a measurement of a leakage channel fiber [11] provided by Prof. L. Dong's research group at Clemson University. This fiber was measured with the aid of an infrared camera at a measurement wavelength of 2000 nm because the very large refractive index contrast ($\Delta n \sim 0.02$) between the cladding (*yellow/red*) and the low-

index regions (*blue*) produced strong phase ambiguities at shorter wavelengths. The phase ambiguities are responsible for the approximately radial measurement artifacts particularly evident at large radius.

Figure 2(e) depicts a zoomed-in measurement of a stress-birefringent air-silica microstructured fiber at 632.8 nm (*NKT Photonics* LMA-PM-10 purchased from *Thorlabs*). Although this result also shows phase ambiguity artifacts, the irregular, angular boundary of the stress rods (large blue features) are accurately rendered by the new algorithm. Furthermore, the oil-infused airholes at the center of the domain are depicted with micron-scale resolution. The slight angular displacement between the orientation of the stress rods and that of the microstructure is real.

In summary I have described details of a new multifocus tomography algorithm that is particularly effective for characterizing multi-core and microstructured optical fibers since they typically contain fine details far from the fiber's center. Although it was validated here by interferometric refractive index measurements, this new algorithm is effective for all types of transverse fiber measurements including non-interferometric refractive index measurement, residual stress measurement and spontaneous emission measurement.

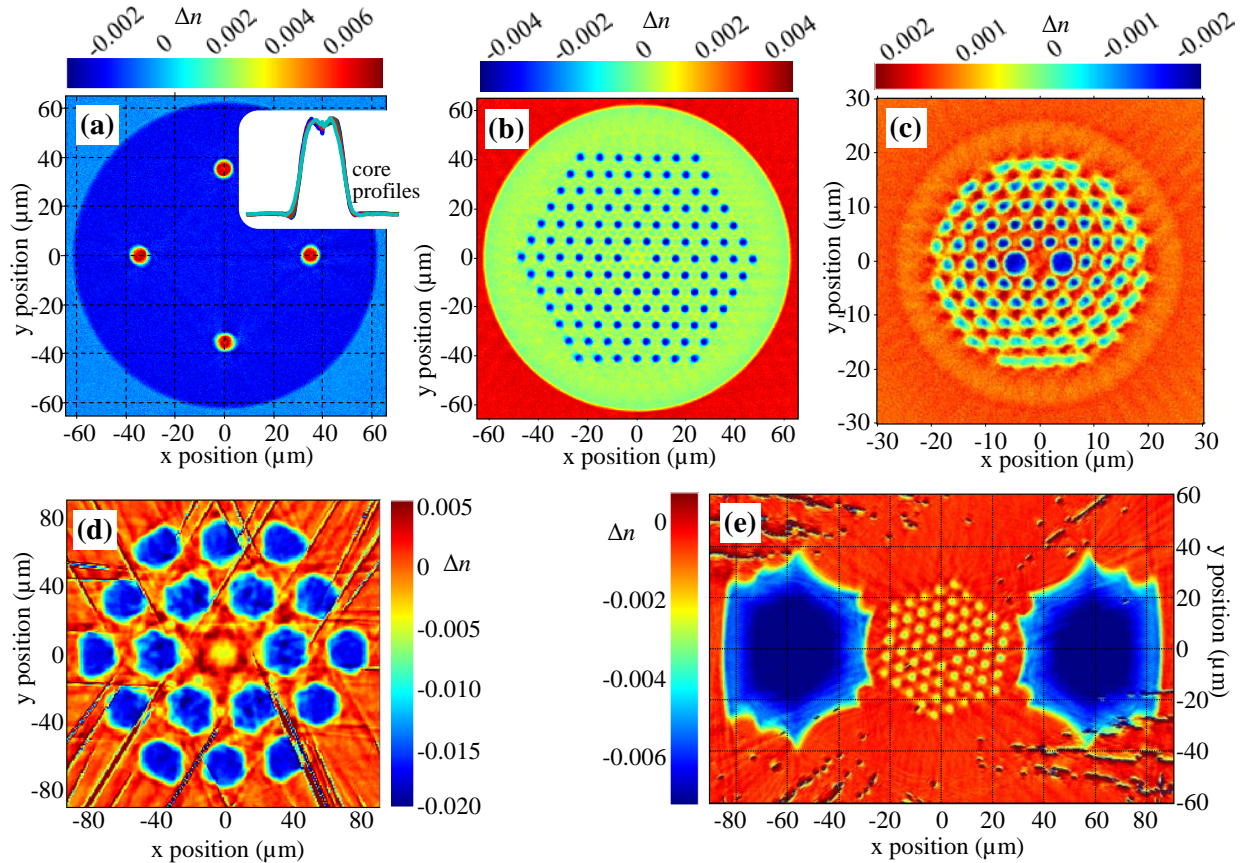


Fig. 2. Refractive index measurements obtained using new algorithm on (a) *Fibercore* FM 4C1500 at 850 nm; (b) *NKT Photonics* ESM-12B purchased from *Thorlabs* measured at 632.8 nm; (c) *NKT Photonics* PM-1550 purchased from *Thorlabs* measured at 632.8 nm; (d) leakage channel fiber (LCF) provided by Liang Dong at Clemson University measured at 2000 nm; (e) *NKT Photonics* LMA-PM-10 purchased from *Thorlabs* measured at 632.8nm. False color scales, which differ amongst the plots, are shown adjacent to each, and depict Δn , the refractive index difference between fiber and surrounding oil.

4. References

- [1] A. Barty, K.A. Nugent, A. Roberts, A. and D. Paganin, *Optics Communications* **175**, 329-336 (2000).
- [2] B. L. Bachim and T.K. Gaylord, *Appl Opt* **44**, 316-327 (2005) and B. L. Bachim, T.K. Gaylord, S.C. Mettler, *Opt Lett* **30**, 1126-1128 (2005).
- [3] W. Gorski and W. Osten, *Optics Letters* **32**, 1977-1979 (2007).
- [4] N. M. Dragomir, X. M. Goh, and A. Roberts, *Microscopy Res and Technique* **71**, 5-10 (2008).
- [5] P. Kniazewski, T. Kozacki, and M. Kujawinska, *Optics and Lasers in Engineering* **47**, 259-263 (2009).
- [6] A. D. Yablon, *IEEE Journal of Lightwave Technology* **28**, 360-365 (2010).
- [7] A. D. Yablon, *Optical Engineering* **50**, 11603 (2011).
- [8] M. Jenkins and T. K. Gaylord, "3D Characterization of the Refractive-Index and Residual-Stress Distributions in Optical Fibers," in *Frontiers in Optics 2012/Laser Science XXVIII*, OSA Technical Digest (online) (Optical Society of America, 2012), paper FTh3C.2.
- [9] A.C. Kak and M. Slaney, *Principles of Computerized Tomographic Imaging* (SIAM, 2001), Chapter 3.
- [10] A.D. Yablon, "Multi-Focus Tomographic Algorithm for Measuring Optically-Thick Specimens," accepted for publication in *Opt Lett*, 2013.
- [11] G. Gu, F. Kong, T.W. Hawkins, P. Foy, K. Wei, B. Samson, and L. Dong, *Optics Express* **21**, 24039-24048 (2013).